Title

Fast 3D T2 -weighted imaging using variable flip angle transition into driven equilibrium (3D T2 -TIDE) balanced SSFP for prostate imaging at 3T.

Journal

Magnetic resonance in medicine, 74(2)

ISSN

0740-3194

Authors

Srinivasan, Subashini
Wu, Holden H
Sung, Kyunghyun
et al.

Publication Date

2015-08-01

DOI

10.1002/mrm.25430

Peer reviewed

Fast 3D T_2-Weighted Imaging Using Variable Flip Angle Transition into Driven Equilibrium (3D T_2-TIDE) Balanced SSFP for Prostate Imaging at 3T

Subashini Srinivasan,[1,2] Holden H. Wu,[1,2,3] Kyunghyun Sung,[1,2] Daniel J.A. Margolis,[1] and Daniel B. Ennis[1,2,3]*

Purpose: Three-dimensional (3D) T_2-weighted fast spin echo (FSE) imaging of the prostate currently requires long acquisition times. Our objective was to develop a fast 3D T_2-weighted sequence for prostate imaging at 3T using a variable flip angle transition into driven equilibrium (T_2-TIDE) scheme.

Methods: 3D T_2-TIDE uses interleaved spiral-out phase encode ordering to efficiently sample the k_y–k_z phase encodes and also uses the transient balanced steady-state free precession signal to acquire the center of k-space for T_2-weighted imaging. Bloch simulations and images from 10 healthy subjects were acquired to evaluate the performance of 3D T_2-TIDE compared to 3D FSE.

Results: 3D T_2-TIDE images were acquired in 2:54 minutes compared to 7:02 minutes for 3D FSE with identical imaging parameters. The signal-to-noise ratio (SNR) efficiency was significantly higher for 3D T_2-TIDE compared to 3D FSE in nearly all tissues, including periprostatic fat (45 ± 12 vs. 31 ± 7, $P < 0.01$), gluteal fat (48 ± 8 vs. 41 ± 10, $P = 0.12$), right peripheral zone (20 ± 4 vs. 16 ± 8, $P = 0.12$), left peripheral zone (17 ± 2 vs. 12 ± 3, $P < 0.01$), and anterior fibromuscular stroma (12 ± 4 vs. 4 ± 2, $P < 0.01$).

Conclusion: 3D T_2-TIDE images of the prostate can be acquired quickly with SNR efficiency that exceeds that of 3D FSE. **Magn Reson Med 74:442–451, 2015. © 2014 Wiley Periodicals, Inc.**

Key words: 3D T_2-weighted imaging; variable flip angle; 3D prostate imaging; 3D T_2-TIDE

INTRODUCTION

T_2-weighted prostate MRI is the clinical standard for anatomic imaging of prostate (1) and is routinely performed using fast spin echo techniques (i.e., fast spin echo [FSE], turbo spin echo, or rapid acquisition with relaxation enhancement). Three-dimensional (3D) T_2-weighted prostate imaging is preferred for imaging small tumors and for acquiring near isotropic slices that are amenable to multiplanar reformatting, which is useful for multimodal registration applications during biopsy, surgical, or treatment planning (2).

The conventional 2D FSE sequences use a series of 180° refocusing pulses with a long repetition time (TR) for signal recovery to produce purely T_2-weighted images. The use of 180° pulses increases the specific absorption rate (SAR) of the sequence, especially at 3T, and the number of acceptable refocusing pulses is further limited due to fast signal decay and concomitant image blurring. These disadvantages can be overcome by lowering the refocusing flip angles (FAs) (3–4) or by designing variable flip angle (VFA) schemes that modulate the refocusing FA train for T_2-weighted FSE (5–7). However, 3D T_2-weighted FSE prostate imaging can take over 7 minutes to acquire, even with a VFA scheme.

Balanced steady state free precession (bSSFP) imaging is widely used for numerous clinical applications due to its high signal-to-noise ratio (SNR) efficiency. However, the steady state signal of bSSFP is T_2/T_1 weighted, which is not desirable for clinical applications in which the underlying abnormality may vary in both T_1 and T_2. Two-dimensional single-shot T_2-weighted imaging has previously been demonstrated using SSFP techniques such as 2D T_2-transition into driven equilibrium (TIDE) (8) and 2D T_2 variable amplitude PSIF (9) based on the TIDE sequence (10). In these approaches the T_2-weighted signal is obtained by acquiring the central k-space lines during the transient state of the SSFP magnetization using FA = 180°, followed by ramping down the FA to a lower FA while acquiring the outer k-space lines to reduce the overall SAR and maintain the sharpness of the reconstructed image. The T_2 weighting in these techniques is controlled by the initial number of 180° pulses and the partial Fourier factor, similar to 2D single-shot half-Fourier acquisition single-shot turbo spin-echo (HASTE) imaging (11). Extension of these techniques to 3D encoding schemes, however, is not practical because of the SAR limitation that arises from the long acquisition durations, especially with a short TR at higher field strengths ($\geq$ 3T).

Our objective was to overcome these limitations by developing and evaluating a novel method for fast 3D T_2-weighted TIDE (3D T_2-TIDE) bSSFP imaging with application to prostate imaging at 3T. Three-dimensional T_2-TIDE uses a VFA scheme similar to 2D T_2-TIDE to reduce the SAR and maintain the T_2 weighting by acquiring the central k-space lines first during the

[1]Department of Radiological Sciences, University of California, Los Angeles, California, USA.

[2]Department of Bioengineering, University of California, Los Angeles, California, USA.

[3]Biomedical Physics Interdepartmental Program, University of California, Los Angeles, California, USA.

*Correspondence to: Daniel B. Ennis, Ph.D., Peter V. Ueberroth Building, Suite 1471, Room B 10945 Le Conte Avenue, Los Angeles, CA 90095. E-mail: daniel.ennis@ucla.edu.

Received 5 April 2014; revised 5 August 2014; accepted 6 August 2014
DOI 10.1002/mrm.25430
Published online 5 September 2014 in Wiley Online Library (wileyonlinelibrary.com).

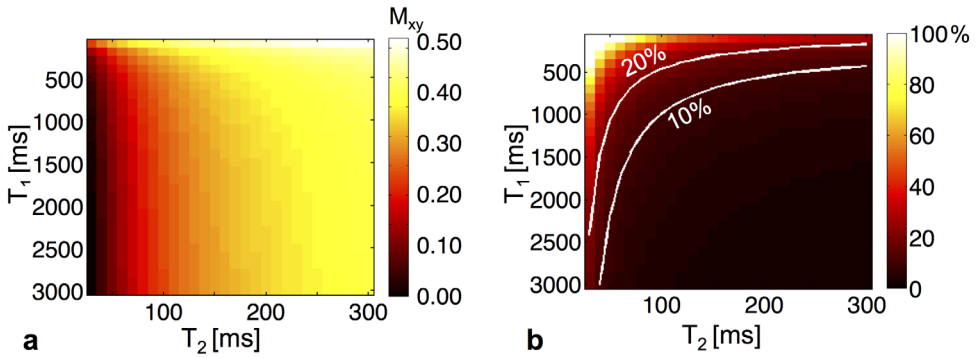

FIG. 1. (**a**) The simulated signal of the 50th echo and flip angle = 60° for a range of T_1s from 100 ms to 3000 ms in steps of 100 ms and range of T_2s from 30 ms to 300 ms in steps of 50 ms. (**b**) The percent signal difference between the signal in (a) and pure T_2 decay simulated with a long $T_1 = 10^9$ ms for all the T_2s. (b) Shows that for tissues with long T_1s, the T_2 weighting is similar to pure T_2 decay. However, as T_1s and T_2s become shorter, the T_2 weighting of the signal decreases.

transient state with a FA lower than 180°, followed by ramping down to a lower FA while acquiring the outer k-space lines. The 3D T_2-TIDE images are acquired faster than 3D FSE by using a spiral-out phase encode ordering in the k_y–k_z plane of the 3D Cartesian k-space trajectory (12) to efficiently sample the central 3D k-space lines with T_2 weighting. Image sharpness is improved by implementing a multishot interleaved acquisition scheme. This k-space acquisition scheme also eliminates the need for partial Fourier acquisitions to control the T_2 weighting, as done for 2D T_2-TIDE or 3D FSE. Furthermore, the acquisition of outer k-space lines with a lower FA steady-state bSSFP approach permits extended echo train durations compared to FSE.

THEORY

The decay of the transient signal (M_{xy}) for on-resonance spins in bSSFP, with perfectly balanced gradients and a preparation pulse of α/2, applied for a duration of TR/2 (13) can be expressed as

$$M_{xy}(n) = \left(\sin\left(\frac{\alpha}{2}\right)M_0 - M_{ss}\right)\lambda^n + M_{ss} \quad [1]$$

where n is the echo number, α is the FA, M_0 is the proton density, M_{ss} is the steady-state bSSFP signal, and the decay rate (λ) of the *transient signal* is given as (13–14)

$$\lambda = E_2 \sin^2(\alpha/2) + E_1 \cos^2(\alpha/2). \quad [2]$$

with $E_{1,2} = \exp(-TR/T_{1,2})$. λ is purely T_2-weighted if α = 180°, but a 180° FA is not practicable for extended echo trains due to SAR limitations. T_2 weighting, however, can also be attained when $TR/T_1 \sim 0$ (i.e., $E_1 \sim 1$). This approximation holds at higher field strengths due to the increased T_1 (15) and when using a short TR, which is preferred when using bSSFP to reduce off-resonance–induced banding artifacts and improve sequence efficiency. Figure 1a shows the simulation of the bSSFP transient signal for the 50th echo with TR = 4.84 ms, echo time (TE) = 2.42 ms, and α = 60° for a broad range of T_1s (100 ms to 3000 ms) and a broad range of T_2s (30 ms to 300 ms). The 50th echo was chosen to demonstrate the achievable signal weighting for the chosen T_2s. Figure 1b shows the percentage of signal change between the simulations shown in Figure 1a and the simulation for the pure T_2 decay signal. The pure T_2 decay signal was simulated for all the T_2s for the 50th echo with α = 60° and a long $T_1 = 10^9$ ms to ensure $TR/T_1 \sim 0$ (i.e., $E_1 \sim 1$). Isocontours (white curves) for 10% and 20% signal differences are highlighted. Note that as T_1 and T_2 decrease, the percentage signal difference becomes larger. For example, the prostate tissues with $T_1 \sim 1500$ ms and $T_2 \sim 50$ ms has a percentage signal difference of 15% for $T_2 = 50$ ms. The decay rate of the transient signal, in the presence of off-resonance, will also be predominantly T_2-weighted for long T_1s (14).

METHODS

3D T_2-TIDE Image Acquisition Scheme

The FA scheme for 3D T_2-TIDE is similar to the 2D T_2-TIDE scheme. Both approaches use preparation pulses to control the T_2 weighting, followed by image acquisition (Fig. 2a). An $\alpha_{high}/2$ preparation pulse is followed by N_{prep} preparation pulses at α_{high} to control the T_2 weighting of the images; increasing N_{prep} increases the T_2 weighting. These N_{prep} pulses are also used for stabilization of the off-resonance signal. This is followed by data acquisition using α_{high} to maintain the T_2 weighting, then smoothly ramped down (10) to a lower FA α_{low}, which reduces SAR. The α_{high} is lower in 3D T_2-TIDE compared to 2D T_2-TIDE ($\alpha_{high} = 180°$) to reduce the SAR for 3D acquisitions, in addition to maintaining the T_2 contrast (see Theory section).

The image acquisition duration of 3D T_2-TIDE is made faster by acquiring the 3D Cartesian k-space in the k_y–k_z plane by utilizing a spiral-out phase encode ordering (12). The acquisition pattern is designed to acquire the 3D central k-space lines with α_{high}, thereby maintaining the T_2 contrast, and moves outward in a spiral pattern to the high spatial frequency k-space lines, which are acquired while the bSSFP signal approaches the steady-state T_2/T_1 weighting. Multishot or interleaved spiral-out phase encode ordering within the k_y–k_z plane is performed to distribute the transition of the transient signal

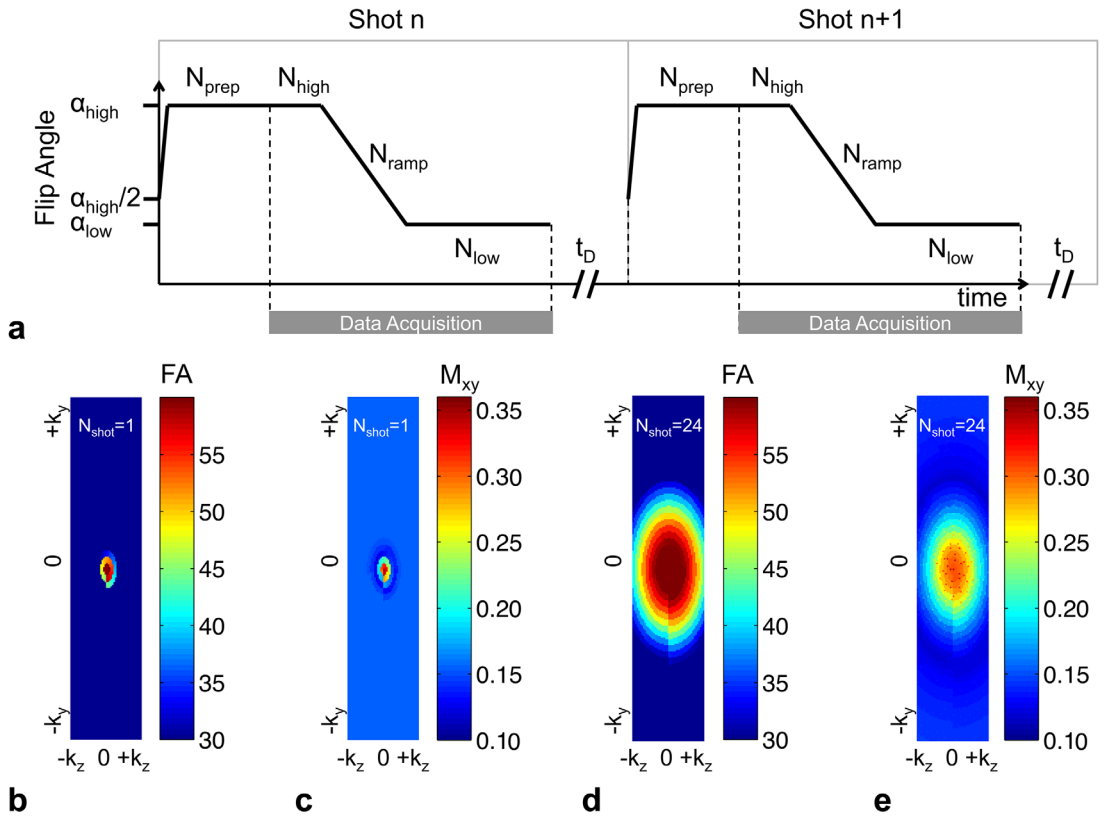

FIG. 2. (**a**) Block diagram showing the FA scheme of the interleaved 3D T_2-TIDE sequence. The $\alpha_{high}/2$ prep pulse is followed by N_{prep} α_{high} preparation pulses to control the T_2 weighting of the image. The images are acquired with N_{high} α_{high} pulses to maintain the T_2 contrast of the image and are smoothly ramped down to α_{low} to reduce the specific absorption rate. A delay of t_D is applied for the recovery of M_z and is followed by the acquisition of the next shot. Simulation of tissue with $T_1/T_2 = 1500/150$ ms and $N_{shot} = 1$ showing the (**b**) FA variation along spiral sampling in ky–kz plane, which generates a (**c**) signal and the corresponding (**d**) FA and (**e**) signal for $N_{shot} = 24$. 3D, three-dimensional; FA, flip angle; TIDE, transition into driven equilibrium.

across a broader range of spatial frequencies, thereby improving the sharpness of the image compared to single-shot approaches, albeit at the cost of increased scan time. The multishot images are acquired by including a time delay (t_D) after each shot, which allows for recovery of the longitudinal magnetization (M_z) before acquisition of the subsequent shot.

Bloch Simulations

In order to understand parameter selection, image contrast, and spatial resolution, Bloch equation simulations of the 3D T_2-TIDE sequence were performed in MATLAB (Mathworks, Natick, MA). Simulations of the transverse magnetization (M_{xy}) for bSSFP were performed for normal prostate tissue with $T_1/T_2 = 1500/150$ ms (16–17), TR/TE = 4.84/2.42 ms, $Nk_y = 230$, $Nk_z = 48$, $\alpha_{high} = 60$, $\alpha_{low} = 30$, $N_{prep} = 50$, $N_{high} = 20$, $N_{ramp} = 200$, and $t_D = 1635$ ms for number of shots (N_{shot}) = 1 and $N_{shot} = 24$. The N_{low} was calculated as $N_{low} = (Nk_y \times Nk_z/N_{shot}) - (N_{high} + N_{ramp})$. For example, for the above mentioned simulation parameters with $N_{shot} = 24$, N_{low} was calculated as 240. These simulation parameters are identical to that of the subsequent 3D T_2-TIDE in vivo imaging experiments (Table 1). The signal profile within the k_y–k_z plane was generated by combining the simulated single-shot or multishot signal with the generated k_y–k_z spiral-out phase encoding trajectory pattern.

The maximum contrast between normal prostate tissue with $T_1/T_2 = 1500/150$ ms and prostate tumor tissue with $T_1/T_2 = 1500/100$ ms (16–17) was determined by performing signal difference simulations with constant FA scheme ($\alpha_{high} = \alpha_{low}$) for a range of α_{high}, varying from 10° to 180° and $N_{prep} = 1$ to 150 with TR/TE = 4.84/2.42 ms. These simulations were performed to determine the N_{prep} required for maximum signal contrast with the maximum achievable α_{high} determined by the SAR limitations.

The T_1 contributions to the 3D T_2-TIDE signal were simulated for prostate tissue with $T_1/T_2 = 1500/150$ ms, muscle tissue ($T_1/T_2 = 900/30$ ms), and fat tissue ($T_1/T_2 = 382/68$ ms with off-resonance of 440Hz) (15) using the imaging parameters identical to the previous simulations. The signal evolution for each echo was compared to pure T_2-weighted simulations with identical T_2s, but with long $T_1 = 10^9$ ms, which ensures $TR/T_1 \sim 0$ (i.e., $E_1 \sim 1$ in Eq. [2]).

The effect of N_{shot} on the point spread function (PSF) was determined by simulating the signal (M_{xy}) for normal prostate tissue using imaging parameters identical to the 3D T_2-TIDE in vivo imaging experiments (Table 1) and $N_{shot} = 1$, 16, 24, and 48. The multishot PSF was

Table 1
Prostate Imaging Parameters for the Different Sequences.

	2D FSE	3D FSE	3D T_2-TIDE	3D bSSFP
Field of view (mm)	200 × 400	200 × 400	200 × 400	200 × 200
Resolution (mm)	0.6 × 0.6 × 3.0	0.9 × 0.8 × 1.5	0.9 × 0.8 × 1.5	0.9 × 0.8 × 1.5
Acquisition matrix	320 × 620	256 × 460	256 × 460	256 × 230
Slice thickness (mm)	3.0	1.5	1.5	1.5
Interpolated slices	20	72	72	72
Acquired slices	20	48	48	48
Bandwidth (Hz/px)	200	315	930	930
Flip angle	90°/150°	90°/110°	VFA	30°–35°
Phase encoding direction	R to L	R to L	R to L	A to P
TR/TE (ms)	4000/101	2200/200	4.84/2.42	4.56/2.28
Echo spacing (ms)	11.2	6.14	4.84	4.56
Echo train length	25	90	370[a]	–
GRAPPA factor/reference lines	2/32	2/24	2/24	–
Partial Fourier	–	~6/8	6/8	–
Averages	2	2	2	1
T_{acq} (min)	3:38	7:02	2:54	0:56
Specific absorption rate (W/kg)	1.5 ± 0.2	1.5 ± 0.2	1.6 ± 0.2	1.8 ± 0.3
Delay time, t_D (ms)	3720	1635	1635	–
N_{shots}	–	96	24	–

Phase encoding direction of A to P indicates anterior to posterior. R to L indicates right to left.
[a]The echo train length of 3D T_2-TIDE does not include the N_{prep} pulses.
2D, two-dimensional; 3D, three-dimensional; bSSFP, balanced steady state free precession; FSE, fast spin echo; GRAPPA, generalized autocalibrating partially parallel acquisitions; TE, echo time; TIDE, transition into driven equilibrium; TR, repetition time.

also compared to the PSF of the 3D steady-state bSSFP signal. The inverse Fourier transform of the signal resulted in the 2D PSF in k_y–k_z plane for each N_{shot}.

In Vivo Imaging

Our institutional review board approved the protocol, and written informed consent was obtained from all subjects prior the imaging. All images were acquired on a 3T scanner (Trio, Siemens Medical Solutions, Erlangen, Germany) using a six-channel anterior coil and a six-channel posterior spine matrix for prostate imaging. Prostate images were acquired in 10 healthy male subjects ($N = 10$, age: 29 ± 5 years) using 3D FSE, 2D multislice FSE, 3D T_2-TIDE, and 3D bSSFP to compare their signal differences. The 3D FSE sequence was acquired using a linear trajectory in k_y–k_z space. In particular, each echo train consisted of acquiring every other k_y for a particular k_z. Both the 3D FSE and 2D multislice FSE used a constant refocusing FA. The imaging parameters for each of these acquisitions are summarized in Table 1. Separate noise scans (18−19) with identical imaging parameters without applied radiofrequency pulses were acquired for 3D FSE and 3D T_2-TIDE sequences to estimate the standard deviation (SD) of the noise for SNR calculations.

Images were also acquired with different $N_{prep} = 10$, 25, 60, and 100 with constant $N_{shot} = 24$ in a subset of five healthy subjects to demonstrate the different T_2 weighting achievable with 3D T_2-TIDE. The dependence of the PSF on N_{shot} was demonstrated by acquiring 3D T_2-TIDE images with different $N_{shot} = 1$, 2, 4, 8, 16, 24, and 48 with constant $N_{prep} = 50$. The other imaging parameters for these acquisitions were identical to the 3D T_2-TIDE acquisition parameters mentioned in Table 1, except the phase encoding direction was changed to anterior to posterior with 0% to 13% phase oversampling based on the subject and without generalized autocalibrating partially parallel acquisitions (GRAPPA), averages, and partial Fourier.

In Vivo Data Analysis

The SNR was calculated as the ratio of the mean signal to SD of the noise from the noise scan (19) in five different regions: periprostatic fat, gluteal fat, left peripheral zone, right peripheral zone, and anterior fibromuscular stroma. The SNR was divided by $\sqrt{\frac{2}{4-\pi}} = 1.53$ to account for the Rayleigh distribution of the noise (20). The regions of interest (ROIs) were drawn in a single slice of the 3D FSE images for each of the 10 healthy subjects and copied to the identical slice in 3D T_2-TIDE and their corresponding noise scans. This was performed by an uroradiologist having read over 1000 prostate MRI studies. The SNR efficiency was calculated as the ratio of the SNR to the square root of the acquisition duration in minutes. The contrast-to-noise ratio (CNR) was calculated between the anterior fibromuscular stroma and the peripheral zone as the difference between their SNR, the anterior fibromuscular stroma being consistently low signal and peripheral zone high signal in normal subjects. The SNR of the peripheral zone was calculated as the average of the SNRs of the left and right peripheral zone. The CNR efficiency was calculated as the ratio of the CNR to the square root of the acquisition duration in minutes. A statistical comparison between the SNR efficiency of the 3D FSE and 3D T_2-TIDE was calculated using a paired Student's *t* test for

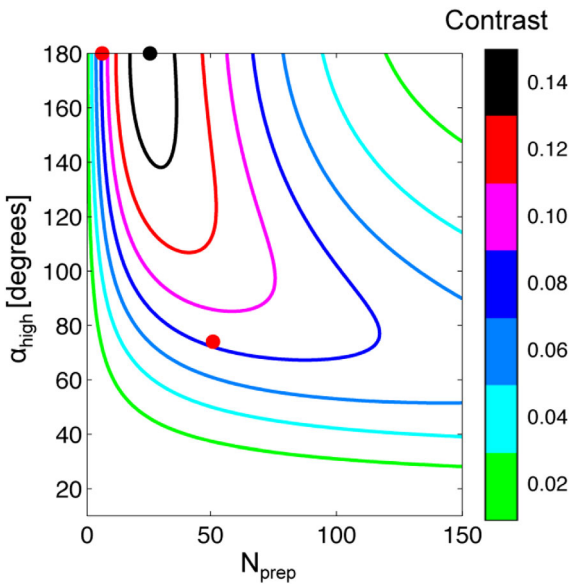

FIG. 3. Simulation of contrast (signal difference) between tissues with $T_1/T_2 = 1500/150$ ms and $T_1/T_2 = 1500/100$ ms for a range of α_{high} from 10° to 180° and a range of N_{prep} from 1 to 150 pulses. The maximum contrast of 0.15 (black dot) achieved by spin echo sequence using α_{high} of 180° and $N_{prep} = 26$, however, cannot be achieved by using a α_{high} lower than 180°. The contrast of 0.08 (red dot) corresponding to spin echo sequence with $\alpha_{high} = 180°$ and $N_{prep} = 7$ can be achieved with a lower $\alpha_{high} = 74°$ with $N_{prep} = 51$ pulses.

the five different regions with $P < 0.05$. The Student's t test values were Holm-Sidak post-hoc corrected.

RESULTS

Simulation Results

Simulated 3D T_2-TIDE images of the signal in the k_y–k_z plane were generated using a VFA scheme (Fig. 2a) with interleaved spiral-out phase encode ordering in the k_y–k_z plane. For simulated prostate tissue, the signal (M_{xy}) in the k_y–k_z plane for $N_{shot} = 1$ and the corresponding VFA scheme (Figs. 2b–c) shows that the center of 3D k-space was acquired with the transient bSSFP signal and the outer k-space lines were acquired while the signal approaches the steady-state bSSFP signal. The corresponding signal and FA scheme for $N_{shot} = 24$ are shown in Figures 2d–e. Multishot 3D T_2-TIDE was used to increase the percentage of the central k_y–k_z phase encodes acquired with the transient signal.

The T_2 contrast of the 3D T_2-TIDE images was governed by the choice of α_{high} and N_{prep}, which were used to specify the VFA scheme. Figure 3 shows the transient bSSFP signal simulation of the contrast between the normal prostate tissue and tumor tissue for a range of α_{high} and N_{prep}. The simulation with $\alpha_{high} = 180°$ corresponds to the T_2 contrast achievable in a spin echo sequence by varying the effective TE (i.e., N_{prep}). The α_{high} used for the 3D T_2-TIDE acquisitions was determined by the SAR limitation at 3T. Hence, for a given α_{high}, N_{prep} can be chosen by following the contrast curve from $\alpha_{high} = 180°$ to the achievable α_{high}. For example, by choosing $\alpha_{high} = 74°$ and $N_{prep} = 51$, contrast of 0.08 is produced, which is also achievable using $\alpha_{high} = 180°$ and $N_{prep} = 7$ (shown as red dots in Fig. 3). The black dot indicates the maximum contrast achieved using $\alpha_{high} = 180°$, which cannot be obtained by using a $\alpha_{high} < 180°$; however, a very similar contrast can be attained with α_{high} as low as 140°.

Figure 4 shows the signal evolution of the transient signal for prostate tissue, muscle, and fat (with off-resonance) and compares their respective signal evolutions to tissues with identical T_2s, but with long $T_1 = 10^9$ ms in order to simulate pure T_2 decay. When $N_{echoes} = N_{prep}$, the transient signal for prostate tissue ($T_1 = 1500$ ms) and muscle ($T_1 = 900$ ms) are similar to the pure T_2 decay due to their long T_1. As a consequence of the short T_1, however, the fat signal ($T_1 = 382$ ms) is higher for 3D T_2-TIDE compared to the pure T_2 decay signal at $N_{echoes} = N_{prep}$.

The PSF of the 3D T_2-TIDE images was improved by increasing N_{shot}. Figures 5a–b shows the simulation of the 2D PSF for $N_{shot} = 1$ and $N_{shot} = 48$. The line profiles along the center of the y- and z-directions for 3D steady-state bSSFP signal, $N_{shot} = 1$, 16, 24, and 48 are shown in Figures 5c–d. The side lobes of the PSF decrease with increasing N_{shot}, which shows that increasing N_{shot} improves the PSF along the y-direction, albeit at the cost of extended scan times. Similar to the y-direction, the side lobes of the multishot acquisitions are attenuated in the z-direction compared to $N_{shot} = 1$. However, the main lobes of the multishot acquisitions are similar to each other.

In Vivo Results

Figure 6 compares axial prostate images acquired in a healthy subject using 3D FSE, 3D T_2-TIDE, 2D multislice FSE, and 3D bSSFP. The 3D T_2-TIDE images are T_2-

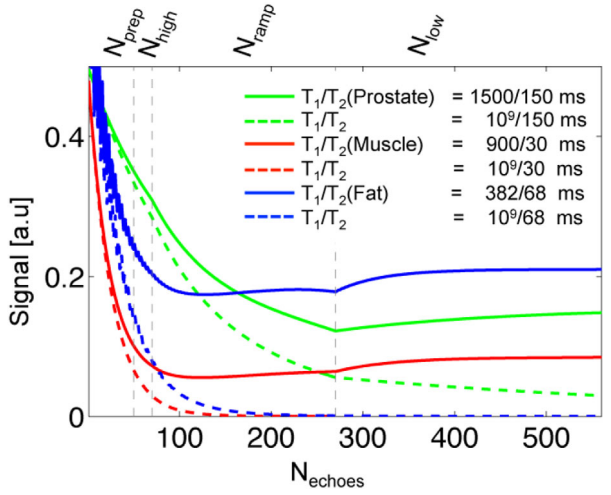

FIG. 4. Signal evolution of prostate tissue (green), muscle (red), and fat (blue) for a single shot with $\alpha_{high} = 60°$, $\alpha_{low} = 30°$, $N_{prep} = 50$, $N_{high} = 20$, and $N_{ramp} = 200$. The fat signal was simulated with an off-resonant frequency of 440 Hz, but the other tissues were simulated at on-resonance. The colored dashed lines represent samples with T_2s identical to the solid colored lines but with long $T_1 = 10^9$ ms.

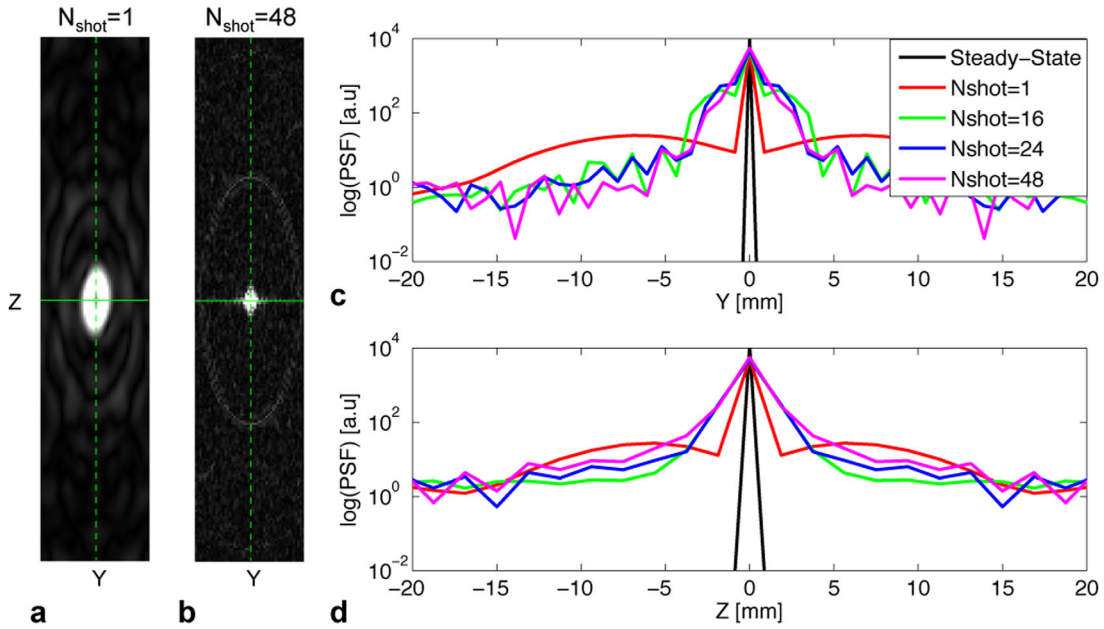

FIG. 5. (**a**–**b**) Image of the 2D PSF for a tissue with $T_1/T_2 = 1500/150$ ms, $Nk_y = 230$, $Nk_z = 48$, $\alpha_{high} = 60°$, $\alpha_{low} = 30°$, $N_{prep} = 50$, $N_{high} = 20$, $N_{ramp} = 200$, and $N_{shot} = 1$, 48. Line profile of the PSF in logarithmic scale along the center in (**c**) *y*- and (**d**) *z*-direction with steady-state signal (black), $N_{shot} = 1$ (red), $N_{shot} = 16$ (green), $N_{shot} = 24$ (blue), and $N_{shot} = 48$ (magenta). Interleaved (multishot) acquisition has reduced side lobes, and thus improved sharpness compared to $N_{shot} = 1$. 2D, two-dimensional; PSF, point spread function.

weighted similar to 3D FSE and 2D multislice FSE, with clear delineation of the prostate "capsule." The acquisition duration of 3D T_2-TIDE was 2:54 minutes compared to the 3D FSE acquisition duration of 7:02 minutes. Compared to the T_2-weighted images, the 3D bSSFP images show that the contrast between the anterior

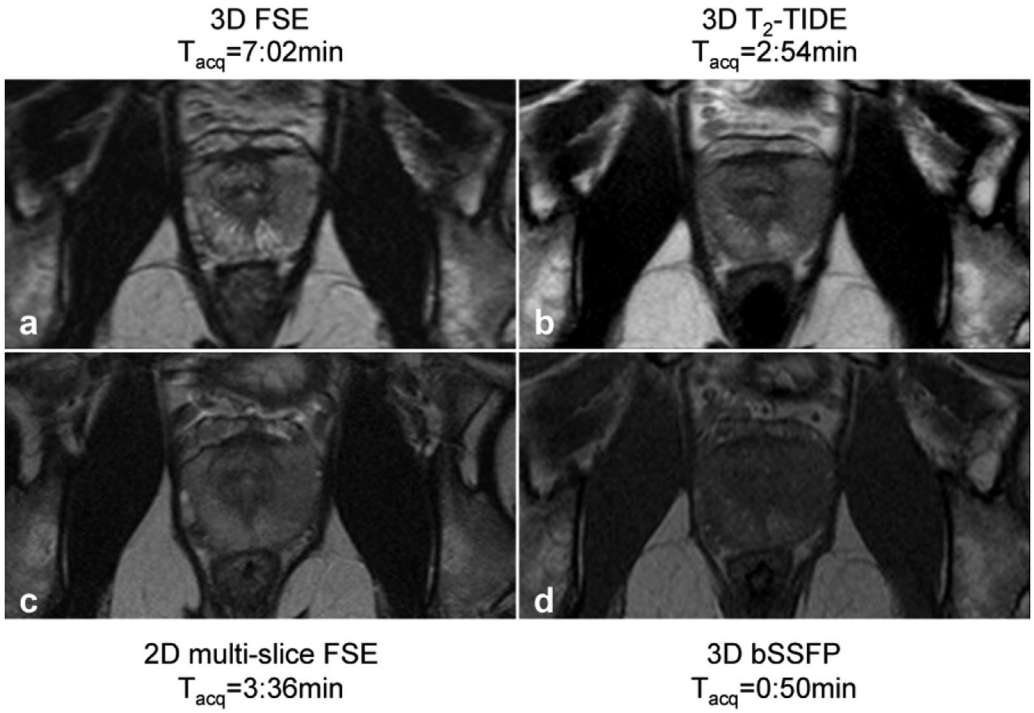

FIG. 6. Single slice images of a healthy subject using (**a**) clinical 3D FSE, (**b**) 3D T_2-TIDE, (**c**) 2D multislice FSE, and (**d**) 3D bSSFP. The 3D T_2-TIDE images are T_2-weighted similar to 3D FSE and 2D multislice FSE with clear delineation of the prostate "capsule." However, in 3D bSSFP, the contrast between the anterior fibromuscular stroma and the peripheral zone and tissue signal heterogeneity within the prostate are qualitatively reduced. 3D, three-dimensional; bSSFP, balanced steady state free precession; FSE, fast spin echo; TIDE, transition into driven equilibrium.

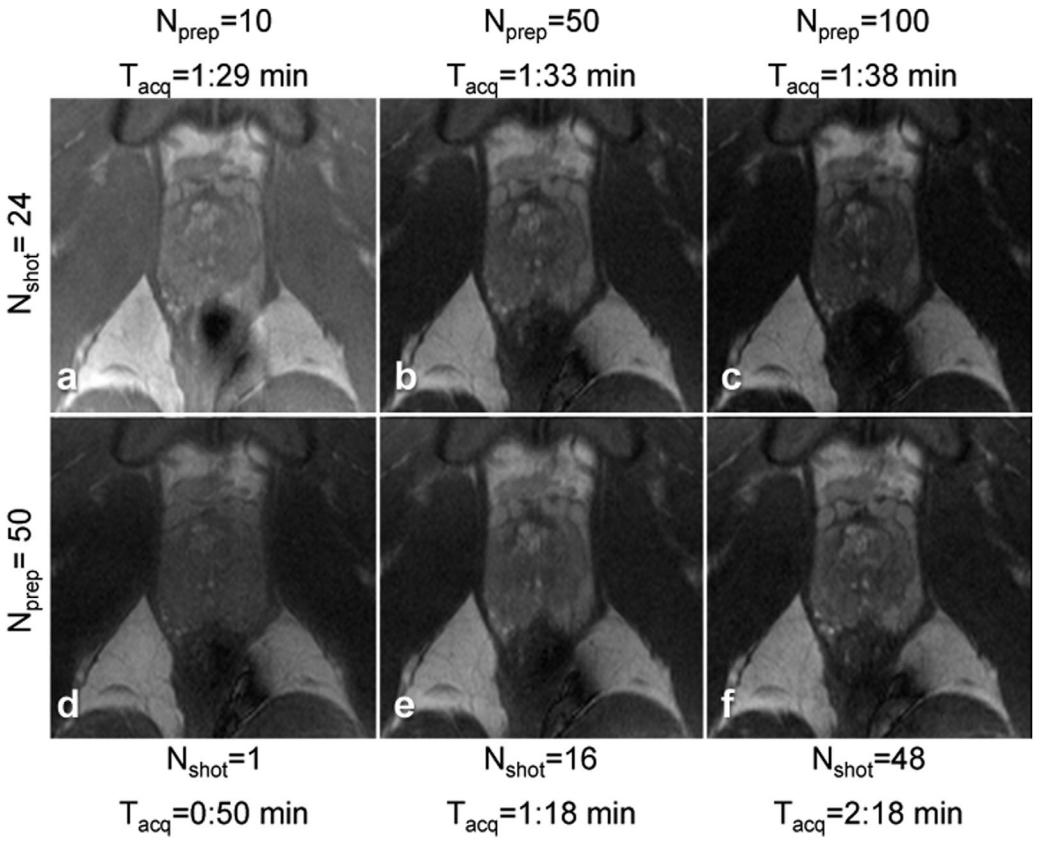

FIG. 7. Single slice from 3D T_2-TIDE images from a healthy subject showing the differences in T_2 weighting due to (**a**) $N_{prep} = 10$, (**b**) $N_{prep} = 50$, and (**c**) $N_{prep} = 100$ with constant $N_{shot} = 24$. Higher N_{prep} results in increased T_2 weighting. The images in the bottom row show the change in the sharpness of the image due to (**d**) $N_{shot} = 1$, (**e**) $N_{shot} = 16$, and (**f**) $N_{shot} = 48$ with constant $N_{prep} = 50$. Higher N_{shot} results in sharper images due to the improvement in PSF. All the images have the same window level. 3D, three-dimensional; PSF, point spread function; TIDE, transition into driven equilibrium.

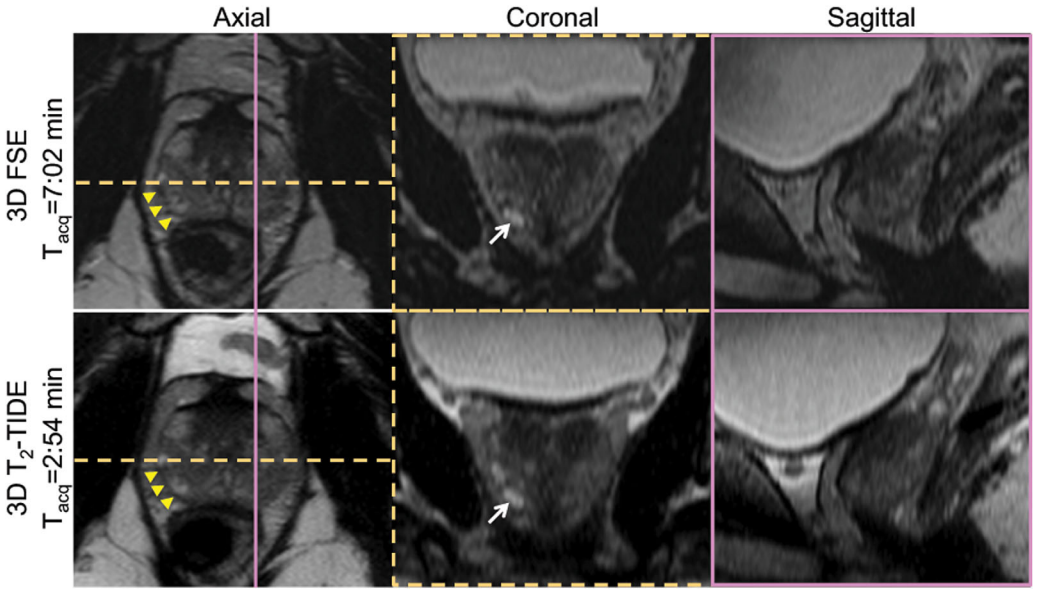

FIG. 8. Three-dimensional FSE (top row) and 3D T_2-TIDE (bottom row) acquired in axial plane in a healthy subject showing clear delineation of the prostate capsule (yellow arrows). The reformatted images in the coronal and sagittal plane also show good definition of features such as cystic benign nodule (white arrow) within the prostate. 3D, three-dimensional; FSE, fast spin echo; TIDE, transition into driven equilibrium.

Table 2
Comparison of SNR and SNR Efficiency Acquired Using 3D T_2-TIDE and 3D FSE in Five Different Regions

	Periprostatic Fat	Gluteal Fat	Right Peripheral Zone	Left Peripheral Zone	Anterior Fibromuscular Stroma
SNR					
3D T_2-TIDE	118 ± 31	124 ± 21	51 ± 10	45 ± 6	31 ± 10
3D FSE	125 ± 27	168 ± 7	64 ± 34	50 ± 12	14 ± 7
P	0.48	< 0.01	0.17	0.19	< 0.01
SNR Efficiency					
3D T_2-TIDE	45 ± 12	48 ± 8	20 ± 4	17 ± 2	12 ± 4
3D FSE	31 ± 7	41 ± 10	16 ± 8	12 ± 3	4 ± 2
P	< 0.01	0.12	0.12	< 0.01	< 0.01

3D, three-dimensional; FSE, fast spin echo; SNR, signal-to-noise ratio; TIDE, transition into driven equilibrium.

fibromuscular stroma and the peripheral zone and tissue signal heterogeneity within the prostate are qualitatively reduced.

Figures 7 a–c shows 3D T_2-TIDE images acquired with constant $N_{shot} = 24$ and different T_2 weighting by changing $N_{prep} = 10$, 50, and 100. Lower N_{prep} results in reduced T_2 contrast with similar image sharpness, whereas increasing N_{prep} improves T_2 contrast. All images have the same window level. Figures 7 d–f shows 3D T_2-TIDE images acquired with varying $N_{shot} = 1$, 16, and 48 and constant $N_{prep} = 50$. The delineation of the prostate capsule is improved with increasing N_{shot} due to improvement in the PSF, but with a penalty of increased acquisition duration, as shown in each figure.

Figure 8 compares the acquisition of 3D T_2-TIDE to 3D FSE for images acquired in the axial plane and reformatted into the coronal and sagittal planes. Overall, the image quality and contrast are very similar, but the 3D T_2-TIDE images are acquired significantly faster. In particular, note that the prostate capsule is clearly depicted in both of these acquisitions in all the imaging planes. The isovolumetric resolution allows for improved fidelity in multimodal image fusion, and multiplanar reformations may obviate the need for acquisition of additional pulse sequences to visualize those planes.

The SNR and the SNR efficiency of 3D T_2-TIDE were compared to 3D FSE in five different regions from images acquired in the healthy subjects ($N = 10$), which are summarized in Table 2. The SNR of gluteal fat was significantly lower in 3D T_2-TIDE, and the SNR of the anterior fibromuscular stroma was significantly higher in 3D T_2-TIDE compared to 3D FSE. The SNR efficiency of the anterior fibromuscular stroma, periprostatic fat, and left-peripheral zone was significantly higher in 3D T_2-TIDE compared to 3D FSE. The CNR between the anterior fibromuscular stroma and peripheral zone using 3D T_2-TIDE was 17 ± 9, and for 3D FSE it was 43 ± 22 ($P < 0.01$). The CNR efficiency between the anterior fibromuscular stroma and peripheral zone using 3D T_2-TIDE was 10 ± 6, and for 3D FSE it was 16 ± 8 ($P = 0.03$).

DISCUSSION

Three-dimensional T_2-TIDE was developed and evaluated for fast 3D T_2-weighted prostate imaging at 3T. We demonstrated that images with an acquisition duration of 2:54 minutes compared very favorably to 3D FSE, with an acquisition duration of 7:02 minutes and matched imaging parameters. The 3D T_2-TIDE images were acquired during the transient state of the bSSFP signal to control the T_2 weighting with multishot spiral-out phase encode ordering in the k_y–k_z plane of the 3D Cartesian trajectory, which enabled acquisition of the central k-space during the transient signal and the outer k-space during the approach to the steady state of bSSFP. This approach balanced maintaining T_2 weighting, preserving image resolution, and scanning fast.

In principle, pure T_2 weighting (identical to a spin echo) is possible with bSSFP imaging during the transient state with $FA = 180°$. Three-dimensional imaging with $FA = 180°$ for extended echo trains with short TRs; however, is not possible at high field strengths ($\geq$ 3T) due to the SAR limitation. Three-dimensional T_2 weighting is still possible with $FA < 180°$ if the tissue T_1 is long compared to TR. Bloch simulation with $FA = 60°$ (Figs. 1a–b) showed that the images will be T_2-weighted for long T_1s with minimal percentage signal difference compared to pure T_2-weighted signal. When both the T_1 and T_2 shorten, the T_2 contrast between tissues decreases. Hence, it may be preferable to acquire 3D T_2-TIDE images precontrast.

The 3D T_2-TIDE signal profile in the first shot is higher than the signal profile in the subsequent shots, which is visible in the signal simulation of $N_{shot} = 24$ as speckles in Figure 2e. This occurs because of the duration required for the 3D T_2-TIDE signal to reach a dynamic steady state between the shots (21–22). The effect of the high signal in the first shot compared to the subsequent shots was analyzed by acquiring 3D T_2-TIDE prostate images in healthy subjects using a discarded preparation shot. These images were compared to identical 3D T_2-TIDE acquisitions without discarding the first shot, and no qualitative effects on the image quality were observed. Thus, all the 3D T_2-TIDE in vivo images was acquired without the discarded shot in order to scan faster.

The maximum T_2 contrast achieved with $\alpha_{high} = 180°$ will be higher than the maximum contrast that is achieved using a lower FA ($\alpha_{high} = 60°$) (Fig. 3). Hence, the CNR and the CNR efficiency between the anterior fibromuscular stroma and the peripheral zone was reduced using 3D T_2-TIDE ($\alpha_{high} = 60°$) compared to 3D FSE ($\alpha = 110°$). However, there was no apparent loss of

signal difference between the peripheral zone and either the anterior fibromuscular stroma or capsule.

The 3D T_2-TIDE images were acquired during the transient state of the bSSFP signal to maintain the T_2 contrast. However, because the signal is not constant during the k-space filling, the PSF of 3D T_2-TIDE is broader compared to the 3D bSSFP imaging (Figs. 5c–d). The PSF is also dependent on the N_{shot} and the spiral-out phase encode trajectory pattern in the Cartesian k_y–k_z plane. Due to the lower resolution along the *z*-direction compared to the *y*-direction, the choice of N_{shot} impacts the PSF along *y* and *z* differently (Figs. 5c–d). Different algorithms can be used to design the sampling pattern for the spiral-out trajectory on the k_y–k_z Cartesian grid, which may improve the PSF in the *y*- and *z*-direction uniformly. Worters et al. (23) have used Bloch simulations for designing a VFA scheme that produces constant bSSFP transverse magnetization. Similar simulations may be used to design VFA schemes that reduce the slope of transient bSSFP signal for 3D T_2-TIDE imaging, thereby improving the PSF. The 2D PSF of 3D T_2-TIDE may be blurred further with partial Fourier acquisitions, and the Bloch simulations did not consider the effects of acquiring data with partial Fourier or GRAPPA.

The 3D FSE sequences used a GRAPPA factor of 2, which permitted acquiring more echoes before the center of k-space (larger partial Fourier factor) and concomitantly reduced image blurring for a fixed echo train duration. The SNR reduction due to parallel imaging in 3D FSE was compensated by averaging twice. Hence, the T_2 weighting in 3D FSE sequences is mainly controlled by the partial Fourier factor and parallel imaging factors. In 3D T_2-TIDE, however, the T_2 contrast is controlled by N_{prep} and does not depend on the parallel imaging and partial Fourier factors. Herein, the in vivo 3D T_2-TIDE experiments used both partial Fourier and parallel imaging factors identical to 3D FSE for fair comparison of acquisition duration and SNR between these sequences.

A low number of Kaiser Bessel (KB) (24) pulses can also be used as preparation pulses instead of the $\alpha_{high}/2$ preparation pulse. Additional simulations are required to determine the number of required KB and N_{prep} pulses, an increased number of KB pulses will reduce the transient signal and/or T_2 weighting. The signal during the N_{prep} prep pulses could also be used to acquire the outer k-space lines for more efficient sampling.

The spiral-out phase encode ordering in the k_y–k_z Cartesian plane of 3D T_2-TIDE enables the use of $N_{shot} \leq N_{kz}$, unlike other conventional 3D linear techniques using $N_{shot} \geq N_{kz}$. For example, if the N_{shot} is decreased, the images can be acquired even faster, however, at the cost of broader PSF or increased image blurriness. This may be useful for monitoring 3D T_2 changes during interventional procedures. If VFA schemes for 3D FSE can be optimized to increase the echo train duration and be combined with phase encode ordering similar to 3D T_2-TIDE, then comparable image contrast and acquisition duration may be possible.

Prostate images are clinically acquired in the axial plane with phase encoding along the right-to-left (RL) direction to reduce rectal motion artifacts, which occur predominantly in the anterior to posterior (AP) direction. As the field of view (FOV) in RL direction is ~2× larger than the FOV in the AP direction, the acquisition duration for the 3D prostate imaging is nearly doubled compared to swapping the phase and frequency axes. If the phase encoding duration is chosen to be along the AP direction, then the acquisition duration of 3D T_2-TIDE can be further reduced to 1:33 minutes (Fig. 7b), which may reduce the prevalence of the apparent rectal motion artifacts and may limit the need for glucagon.

In this paper, 3D T_2-TIDE has been applied for fast 3D T_2-weighted imaging of the prostate. Further evaluation is needed for different applications of 3D T_2-weighted imaging, including the abdomen, breast, uterine tumors (25–26), spine (27), ganglion cysts (28), and ankle.

Limitations

The T_2 contrast in the 3D T_2-TIDE images is due to the acquisition of central k-space lines during the transient bSSFP signal, which is T_2-weighted for a range of T_1s and T_2s, based on the assumption that the image contrast is mainly contributed by the central k-space. This is especially true for large objects approaching the size of the FOV. However, when the object size decreases in the image domain, the central region of k-space that contributes to image contrast increases. Hence, especially for small prostate tumors, the image contrast is due to both the transient signal and the steady-state signal. This property of 3D T_2-TIDE is similar to other VFA acquisition techniques that use higher FAs to acquire the center of the k-space and lower FAs for the outer k-space lines. Furthermore, with regards to image contrast, the T_2 weighting in 3D T_2-TIDE is preserved only for a range of T_1s and T_2s. As a result, 3D T_2-TIDE may not produce sufficient T_2 weighting after contrast administration due to the shortening of the T_1.

The 3D T_2-TIDE images are susceptible to off-resonance–induced banding artifacts; therefore, they require the use of shim gradients to reduce B_0 inhomogeneities and a short TR. The prostate images acquired in healthy subjects did not have banding artifacts when using the standard (i.e., *not* patient-specific) shim. Susceptibility artifacts were also subtly pronounced in regions surrounding the rectum in the 3D T_2-TIDE images compared to the 3D FSE.

The interleaved multishot 3D T_2-TIDE acquisition, with spiral-out phase encode ordering in k_y–k_z, improves the PSF by increasing the distribution of the transient signal in the middle of k_y–k_z. However, due to the delay between subsequent shots, any motion that occurs between shots may result in motion artifacts because the central k-space lines are partly acquired with each shot. Further improvements such as oversampling of the central k_y–k_z space may reduce artifacts due to intershot motion.

CONCLUSION

Three-dimensional T_2-TIDE can be used for fast 3D T_2-weighted prostate imaging at 3T with acceptable image quality and ~58% reduction in acquisition duration

compared to 3D FSE. The flexibility afforded by an interleaved shot strategy in 3D T_2-TIDE enables tradeoffs between acquisition speed and image sharpness.

ACKNOWLEDGMENT

The authors are grateful for research support from Siemens Medical Systems.

REFERENCES

1. Barentsz JO, Richenberg J, Clements R, Choyke P, Verma S, Villeirs G, Rouviere O, Logager V, Futterer JJ. ESUR prostate MR guidelines. Eur Radiol 2012;22:746–757.
2. Rosenkrantz AB, Neil J, Kong X, Melamed J, Babb JS, Taneja SS, Taouli B. Prostate cancer: comparison of 3D T2-weighted with conventional 2D T2-weighted imaging for image quality and tumor detection. AJR Am J Roentgenol 2010;194:446–452.
3. Hennig J. Multiecho imaging sequences with low refocusing flip angles. J Magn Reson 1988;78:397–407.
4. Alsop DC. The sensitivity of low flip angle RARE imaging. Magn Reson Med 1997;37:176–184.
5. Hennig J, Weigel M, Scheffler K. Multiecho sequences with variable refocusing flip angles: optimization of signal behavior using smooth transitions between pseudo steady states (TRAPS). Magn Reson Med 2003;49:527–535.
6. Mugler JP, Bao S, Mulkern RV, Guttmann CRG, Robertson RL, Jolesz FA, Brookeman JR. Optimized single-slab three-dimensional spin-echo MR imaging of the brain. Radiology 2000;216:891–899.
7. Busse RF, Hariharan H, Vu A, Brittain JH. Fast spin echo sequences with very long echo trains: design of variable refocusing flip angle schedules and generation of clinical T2 contrast. Magn Reson Med 2006;55:1030–1037.
8. Paul D, Markl M, Fautz H-P, Hennig J. T2-weighted balanced SSFP imaging (T2-TIDE) using variable flip angles. Magn Reson Med 2006; 56:82–93.
9. Srinivasan S, Gilson WD, Flammang A, Paul D, Patil S. Fast, low SAR and off-resonance insensitive T2 weighted variable amplitude PSIF (T2 VAPSIF) imaging. In Proceedings of 20th Annual Meeting of ISMRM, Melbourne, Australia, 2012. p. 290.
10. Hennig J, Speck O, Scheffler K. Optimization of signal behavior in the transition to driven equilibrium in steady-state free precession sequences. Magn Reson Med 2002;48:801–809.
11. Semelka RC, Kelekis NL, Thomasson D, Brown MA, Laub GA. HASTE MR imaging: description of technique and preliminary results in the abdomen. J Magn Reson Imaging 1996;6:698–699.
12. Vogt FM, Eggebrecht H, Laub G, Kroeker R, Schmidt M, Barkhausen J, Ladd SC. High spatial and temporal resolution MRA (TWIST) in acute aortic dissection. In Proceedings of the 15th Annual Meeting of ISMRM, Berlin, Germany, 2007. p. 92.
13. Scheffler K. On the transient phase of balanced SSFP sequences. Magn Reson Med 2003;49:781–783.
14. Schmitt P, Griswold MA, Gulani V, Haase A, Flentje M, Jakob PM. A simple geometrical description of the TrueFISP ideal transient and steady-state signal. Magn Reson Med 2006;55:177–186.
15. de Bazelaire CMJ, Duhamel GD, Rofsky NM, Alsop DC. MR imaging relaxation times of abdominal and pelvic tissues measured in vivo at 3.0 T: preliminary results. Radiology 2004;230:652–659.
16. Liu W, Turkbey B, Sénégas J, Remmele S, Xu S, Kruecker J, Bernardo M, Wood BJ, Pinto PA, Choyke PL. Accelerated T2 mapping for characterization of prostate cancer. Magn Reson Med 2011;65:1400–1406.
17. Fennessy FM, Fedorov A, Gupta SN, Schmidt EJ, Tempany CM, Mulkern RV. Practical considerations in T1 mapping of prostate for dynamic contrast enhancement pharmacokinetic analyses. Magn Reson Imaging 2012;30:1224–1233.
18. Kellman P, McVeigh ER. Image reconstruction in SNR units: a general method for SNR measurement. Magn Reson Med 2005;54:1439–1447.
19. Hu P, Chan J, Ngo LH, Smink J, Goddu B, Kissinger KV, Goepfert L, Hauser TH, Rofsky NM, Manning WJ, Nezafat R. Contrast-enhanced whole-heart coronary MRI with bolus infusion of gadobenate dimeglumine at 1.5 T. Magn Reson Med 2011;65:392–398.
20. Dietrich O, Raya JG, Reeder SB, Reiser MF, Schoenberg SO. Measurement of signal-to-noise ratios in MR images: influence of multichannel coils, parallel imaging, and reconstruction filters. J Magn Reson Imaging 2007;26:375–385.
21. Paul D, Zaitsev M. Improved SNR in linear reordered 2D bSSFP imaging using variable flip angles. Magnetic Resonance Imaging 2009;27:933–941.
22. Srinivasan S, Ennis DB. Variable flip angle balanced steady−state free precession for lower SAR or higher contrast cardiac cine imaging. Magn Reson Med 2014;71:1035–1043.
23. Worters PW, Hargreaves BA. Balanced SSFP transient imaging using variable flip angles for a predefined signal profile. Magn Reson Med 2010;64:1404–1412.
24. Le Roux P. Simplified model and stabilization of SSFP sequences. J Magn Reson 2003;163:23–37.
25. Hori M, Kim T, Onishi H, Ueguchi T, Tatsumi M, Nakamoto A, Tsuboyama T, Tomoda K, Tomiyama N. Uterine tumors: comparison of 3D versus 2D T2-weighted turbo spin-echo MR imaging at 3.0 T—initial experience. Radiology 2011;258:154–163.
26. Agrawal G, Riherd JM, Busse RF, Hinshaw JL, Sadowski EA. Evaluation of uterine anomalies: 3D FRFSE cube versus standard 2D FRFSE. AJR Am J Roentgenol 2009;193:W558–W562.
27. Meindl T, Wirth S, Weckbach S, Dietrich O, Reiser M, Schoenberg SO. Magnetic resonance imaging of the cervical spine: comparison of 2D T2-weighted turbo spin echo, 2D T2*weighted gradient-recalled echo and 3D T2-weighted variable flip-angle turbo spin echo sequences. Eur Radiol 2009;19:713–721.
28. Shahid KR, Spinner RJ, Skinner JA, Felmlee JP, Bond JR, Stanley DW, Amrami KK. Evaluation of intraneural ganglion cysts using three-dimensional fast spin echo-cube. J Magn Reson Imaging 2010; 32:714–718.